Available online at www.sciencedirect.com

ScienceDirect

Procedia Environmental Sciences 6 (2011) 70–87

Procedia Environmental Sciences

Earth System Science 2010: Global Change, Climate and People

Patterns of decadal climate variability and their impact on global rainfall

Peter G. Baines*

Dept. of Civil and Environmental Engineering, University of Melbourne, Melbourne, VIC 3010 Australia

Abstract

An analysis is made of global sea surface temperature (SST) data sets over the past 110 years to determine the principal patterns of climate variability on time scales longer than ENSO, and to relate these to likely dynamical processes. Taking 5-year running means, the most recent versions of the interpolated global data from the UK Hadley Centre and the US NOAA are analysed using singular value decomposition, and described as coherent global patterns that have a physical/dynamical basis. These patterns are: Global Warming, the Pacific Decadal Oscillation, the Atlantic Multi-decadal Oscillation and the Pacific Gyre Oscillation. Each of these patterns, as represented by SST, is described in both data sets with real and complex empirical orthogonal functions, and current understanding of their dynamical basis is described. An example of the use of such patterns is given through an application to the recent trend pattern in global rainfall. Complete agreement between the two SST data sets is lacking, but both agree that major contributors to this rainfall pattern are global warming and the Pacific Decadal Oscillation, where the latter may be regarded as the low-frequency signal of ENSO.

Selection under responsibility of S. Cornell, C. Downy, S. Colston.
Keywords: decadal climate variability; sea surface temperature; rainfall

1. Introduction

Of all the variables that one may use to describe climate, the most important is (probably) sea surface temperature (SST). This is because of its obvious intrinsic direct effect on the local climate, and in addition (i) it gives a measure of heat storage in the ocean, (ii) it has a controlling effect on the surface winds and pressure, and (iii) it has a controlling effect on surface humidity. Since heat storage in the

* Corresponding author. Fax: +61-3-8344-4616
E-mail address: p.baines@unimelb.edu.au.

1878-0296
doi:10.1016/j.proenv.2011.05.008

upper layers of the ocean is so extensive, SST also has a substantial impact on the climate of nearby land areas.

Another advantage of SST is that, despite many imperfections, the data coverage over the globe is better than that for most other variables, with longer records. In this paper, an analysis of climate over the past 110 years is described, based on observations of SST. This is effectively an update and reappraisal of the analysis described by Parker et al. [1], and it is argued that the patterns of variability of SST are becoming more distinct and better related to dynamical processes. These patterns are described in some detail, and some indications of their impact on rainfall and other variables over the past 30 years are then presented.

2. Data sources and analysis

The collection and interpretation of observations over the past 200 years or so now enable the estimation of global SST back to about 1850. This is a challenging task, as data coverage over most of the global ocean is very scarce prior to the advent of satellite coverage in 1979. These estimates have mainly been generated by two separate groups: the Hadley Centre at the Meteorological Office in the UK [2], and Reynolds, Smith and others at NOAA and the University of Maryland in the USA [3]. A third analysis by Kaplan et al. [4] does not include satellite data, and provides a useful contrast.

Each of these two main groups separately compiles the available observations of SST. For the Hadley Centre, the most recent interpolated analysis is HadISST1 [2], and for the US group it is ERSST.v3 (extended range SST version 3 [3]). These groups work independently and differences in their products are mainly due to the differences in their interpolation procedures. Results for the period prior to 1979 (the start of the satellite era) are influenced by correlations observed more recently. Where these two data sets agree, one may have some confidence in the results, though they are not completely independent as each update may be influenced by the progressive results of the other group. Hence these data sets are still subject to further modification and improvement, and there are notable differences between them when analysed on annual and shorter periods. However, for longer periods of interest here there is a broad measure of agreement, as shown below.

Here, these two data sets are each analysed by first taking averages of ‘ENSO-years’, which are defined to be years that begin in June and end the following May. To avoid confusion with years that contain ENSO events, these ENSO-years are here termed ‘E-years’. A five E-year running mean is then taken in each of HadISST1 and ERSST.v3 from June 1900 until May 2009, giving 105 time-points with central years from 1902-2006 (the years containing June). This form of averaging is commonly used in climate studies, and has a spectral response of less than 0.2 for period less than 6 years. It has the advantages (relative to spectral filtering) that it is easily understood and implemented, and can reproduce abrupt changes faithfully. For each data set the temporal mean value at each grid point (shown in Figure 1 for ERSST.v3) is subtracted, and the remainder is subjected to an area-weighted Empirical Orthogonal Function analysis, at 2-degree (latitude and longitude) resolution.

This EOF analysis may be expressed as follows. If the spatial grid points of SST values are placed in one line as a single row vector, values of SST at successive times placed in successive rows give a data matrix R_{ij}, where $i = 1$ to m times (i.e. central E-years), and $j = 1$ to n spatial points. From the Singular Value Decomposition Theorem, the matrix R_{ij} may be expressed uniquely as:

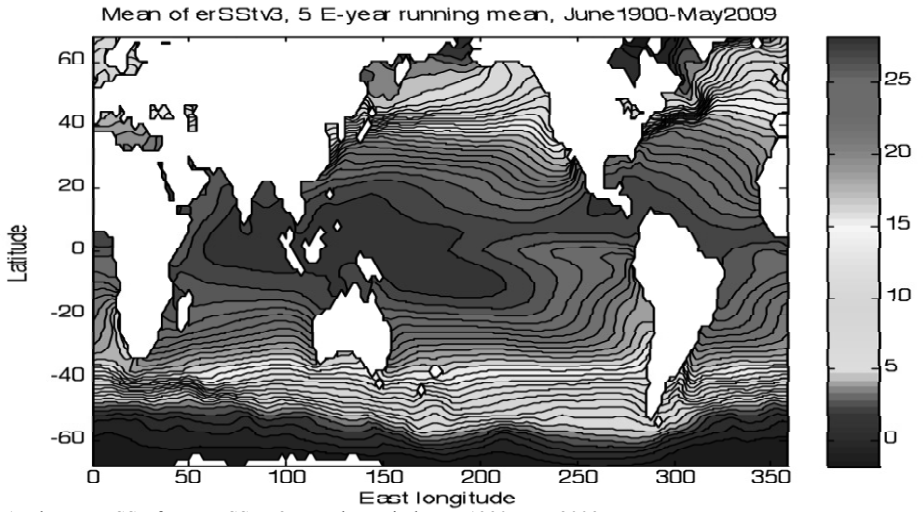

Fig 1. The mean SST from ERSST.v3 over the period June 1990-May 2009.

$$R_{ij} = \sum_{k=1}^{m} S(k,k)U(i,k)V(j,k) \qquad (1)$$

if $m \le n$, where U and V are orthogonal matrices. The data matrix may therefore be expressed as the sum of m (or the minimum of m and n) terms, the kth of which has the form $S(k,k)$ times the kth column of U (a spatial pattern) times the kth row of V (a time series). The value $S(k,k)2$ denotes the variance of this kth EOF, and is usually expressed as a percentage of the total in the data set (i.e. the sum of all of them in the series). Area weighting is represented by multiplying the SST values by the cosine of the latitude before decomposition, and reversing this after. Two regions have been considered and compared: one from 70°N to 70°S latitude, and the other from 70°N to 40°S. This has been done to test the effect of the Southern Ocean – a notoriously poorly observed region – on the analysis. Varimax rotation (Kaiser [5] has also been applied to these data, but no significant difference or benefit was obtained, and the results are not presented here.

The above conventional EOF procedure works well if the data consist of a sum of varying stationary patterns. But if the constituent patterns involve waves propagating through the spatial array, or patterns whose structure varies with time as they go through a cycle, a more appropriate method may be that of complex EOFs. Here the Hilbert transform is taken of the time series $T(\mathbf{r},t)$ at each spatial grid point $\mathbf{r}$, defined by

$$H(T(\mathbf{r},t)) = \frac{1}{\pi} \int_{-\infty}^{\infty} \frac{T(\mathbf{r},t')}{t'-t} \mathrm{d}t, \qquad (2)$$

where the Cauchy principal value of the integral is taken. In general terms, the Hilbert transform of a time series gives a signal that is locally in quadrature with that time series, and hence is out of phase with

it (the Hilbert transform of cost is *sin*t, and of *sin*t, –*cos*t). With a finite data record, the transform is not properly defined near the ends of the range, and this must be allowed for in the interpretation.

This Hilbert transform is now taken to be the imaginary part of the time series at each grid point, so that the total time series is taken to be $T(\mathbf{r},t) + iH(T(\mathbf{r},t))$. One next takes the Singular Value Decomposition of this complex time series in the same way as for the real one. Here the values $S(k,k)$ are still real, but the spatial vectors $U(i,k)$ and time series $V(k,j)$ are both complex, and the matrices U and V are unitary. Physical significance is given to the real part of the resulting decomposition, which involves the product of the real parts of the $U(i,k)$ and $V(k,j)$, plus that of the imaginary parts. The values $S(k,k)^2$ give the fraction of total variance of the complex data, which is the same as the fraction of variance of the real part of this complex data, which is the quantity of interest. If the data set contains variability that is in quadrature with the original real part obtained with conventional EOFs, this procedure identifies it as part of the same pattern. In this case, this should give a more economical and complete description of the data. In practice one may take the complex EOF, and discard it if no benefit accrues, or if the conventional analysis is preferred.

3. Patterns of decadal variability, based on SST.

We next examine the EOFs obtained from this analysis, which we aim to identify as coherent patterns of behaviour with physical or dynamical bases. The extent to which this is justified is discussed in each case.

3.1. EOF1: the Global Warming Pattern

The first EOF in these analyses is shown in Figure 2. Here the spatial pattern of HadISST1 is shown on the left, and that of ERSST.v3 on the right (note different scales), to 70°S for each data set. The corresponding time series are shown in blue for HadISST, and in red for ERSST, with the curves for the region to 70°N-70°S shown as solid, and those for 70°N-40°S shown dashed. This EOF contains more than half the total variance for both data sets, and the difference between the results for 70°N-40°S and 70°S is small. The temporal curves for the four different cases are quite similar, and resemble the mean global warming curve for the planet as a whole ([1], IPCC2007 [6]). The warming since 1950 is generally attributed to the increased concentrations of greenhouse gases in the atmosphere [6]. As such, it is a forced response. The reasons for the behaviour before 1950 where the data are less certain are still controversial. The peak in the early 1940s and sudden decrease in 1945 is apparently due to errors due to changes in temperature measurement (in buckets vs. engine intakes – Thompson et al. [7]), which should be corrected in future releases.

The spatial patterns all indicate approximately spatially uniform increase in SST, though there are localized regions where the two differ – most notably in the North and Central Pacific, where HadISST has two small regions of negative sign. However, they both agree on the negative region in the northern North Atlantic (discussed further below), and (to some extent) on the almost zero change around the coast of Antarctica (which HadISST, being an older analysis, does not fully cover). The latter is not surprising, since the Antarctic continent helps to maintain the mean cold coastal environment. The zonal warming that occurs in the Southern Hemisphere north of about 60°S implies an increase in the north-south temperature gradient to the south, and is related to the increasing strength of the atmospheric Southern Annular Mode (with stronger winds) in this region. Hence, with some regional exceptions (particularly the northern North Atlantic) this spatial pattern is reasonably featureless, and so is the time series for the past 60 years. Indications near the end of the record that the warming is leveling off are not significant, as heat content in the ocean has been accumulating over the past decade, and continues (Lyman et al. [8]).

There is no benefit in taking the complex EOF of this pattern, as it represents an approximately uniform trend (and in consequence its Hilbert transform is dominated by end effects). As such, the real EOF may be subtracted from the record in the same manner as the overall mean, and the analysis is then focused on the variability of the remainder, which is dominated by oscillations and is more susceptible to the complex procedure. Figure 3 shows the percentages of total variance contained in the real EOF analysis (the dashed lines), the real analysis with EOF1 removed (the dotted lines), and the complex EOF analysis with EOF1 removed (solid lines), for both data sets from 70°N-70°S. For EOFs 2, 3 and 4 (with EOF1 removed), the complex analysis (mostly) contains greater fractions of the variance than do the real ones. This implies that the complex analysis provides a better and more complete description of these three patterns. This generally implies that both the real and imaginary parts (of both the spatial patterns and time series) have significant amplitudes, whereas if one or the other is small, the conventional 'standing wave' EOFs may be more appropriate. For the next three patterns the conventional EOFs are first shown, and then the corresponding complex ones.

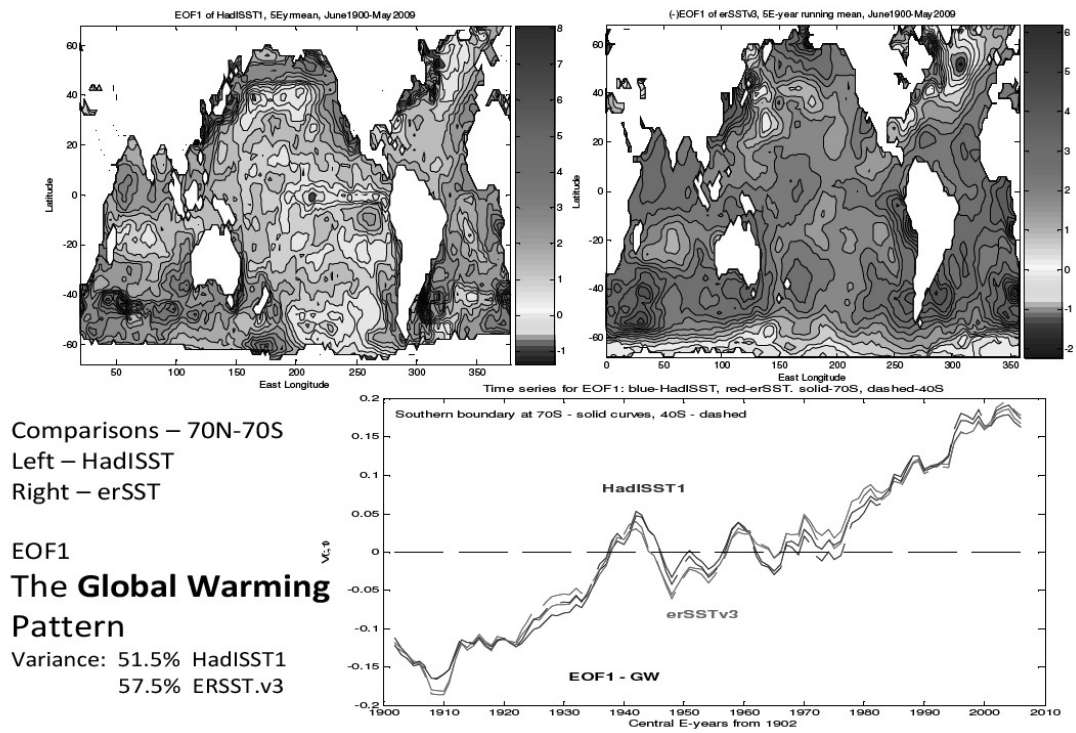

Fig. 2. EOF1 – the Global Warming Pattern. The spatial pattern on the left is for HadISST1, that on the right for ERSST.v3. Blue time series are for HadISST1, red for ERSST.v3, dashed for 70°N-40°S, solid for 70°N-70°S.

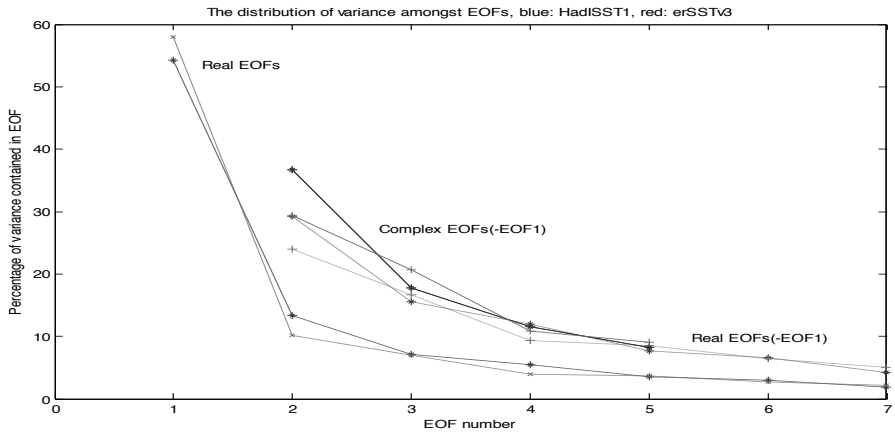

Fig. 3. The percentages of total variance contained in EOFs. The full domain 70N-70S has been used for each. The dashed lines show the percentages for the real EOF analysis (with the mean removed). The dotted lines show the percentages for the real EOF analysis of the data with both the mean and EOF1 (the Global Warming 'trend') removed. The solid lines show the percentages for the complex analysis with the mean and EOF1 removed. Blue denotes HadISST1 data, red denotes erSSTv3 data.

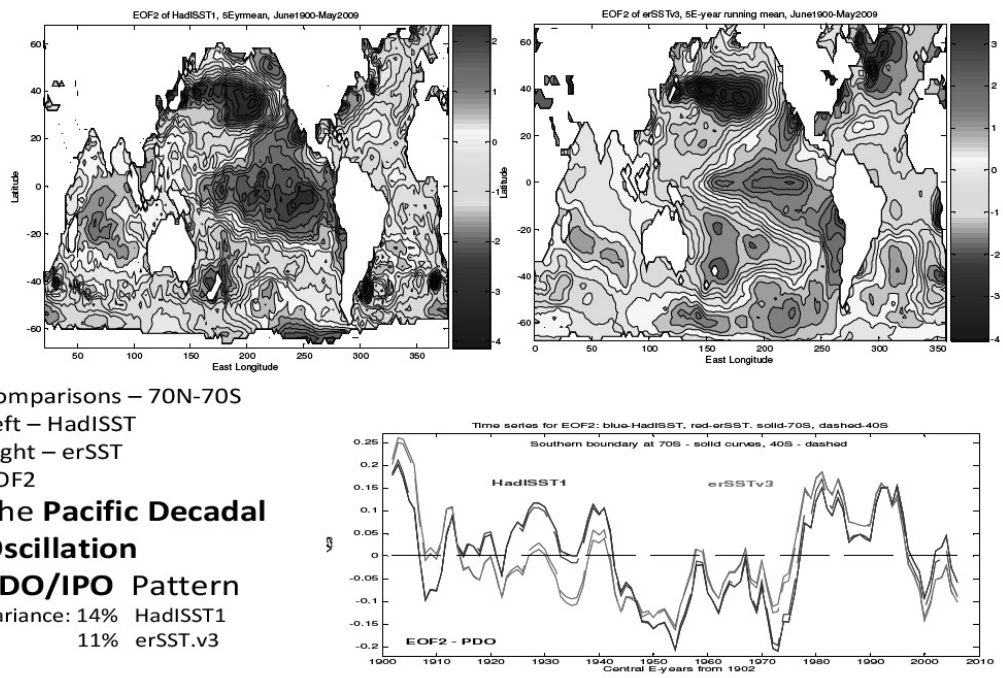

Fig. 4. As for Figure 2, but for the second EOF.

3.2. EOF2: The Pacific Decadal Oscillation

The second conventional EOF is shown in Figure 4. This is generally known as the Pacific Decadal Oscillation (PDO) (Mantua et al. [9]), or the Interdecadal Pacific Oscillation (IPO) (Power et al. [10], the former being a Northern Hemisphere concept, and the latter a pan-Pacific one. Here the main features of the spatial patterns from the two data sets are in reasonable agreement, with the exception at high southern latitudes. The time series for 40S and 70S both agree well for both data sets, and both track the main features of the temporal record, though there is some difference in amplitude prior to 1940. The pattern is dominated by the signal in the North and South Pacific, and has (mostly) smaller amplitude elsewhere.

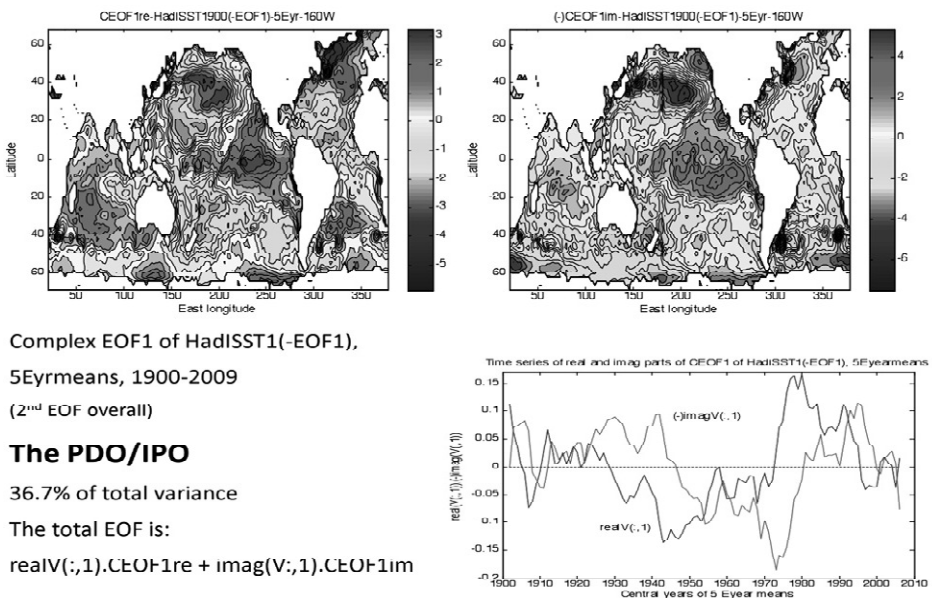

Figure 5. The first complex EOF of HadISST1 data with the mean and first real EOF removed. The total CEOF consists of the spatial pattern on the left times the real time series (in blue), plus the spatial pattern on the right times the imaginary (green) time series.

The first complex EOF (for the PDO/IPO) with the mean and first real EOF (global warming) subtracted, is shown in Figure 5 for HadISST1 data, with the associated time series shown on the complex plane in Figure 6 (the corresponding figures for erSSTv3 are similar, but are omitted to save space). The real and imaginary spatial patterns are not mutually orthogonal, nor are the corresponding time series. The right-hand pattern of Figure 5 has larger variance (0.6) than that on the left (0.4), whereas the variances of the two time series are equal (0.5). Hence the right hand pattern is dominant, and with its time series is seen to be the dominant component, resembling the real EOF2 of Figure 4.

Fig. 6. The time series of CEOF1 on the Argand plane – real part on real axis, imaginary part on imaginary axis.

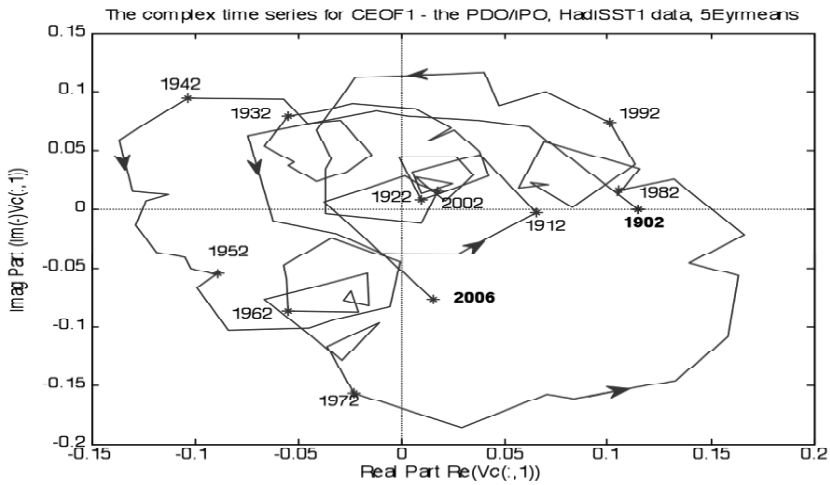

Of all of the first four spatial patterns, this one is probably the least well understood. It is clearly related to ENSO (the El Niño-Southern Oscillation), and contains much of the same physics. However, it is not confined to the tropics, and the positive anomaly in the eastern equatorial Pacific is much more latitudinally extensive than any ENSO event. Debate continues as to whether it is a dynamical entity in itself, or is simply some running average over ENSO events [1]. The fact that the complex analysis gives a better representation than that of the simple EOFs (explaining ~ 5% more variance in each data set) indicates that it has a definite evolving structure, but as Figure 6 shows, there is no dominant periodicity. The system can spend a considerable period of time in a localized region of the diagram, and then move rapidly to another with very different properties. This is consistent with a system that is a sum of random (ENSO) events, or a dynamical entity that is excited by random events. These ENSO events are dependent on mesoscale events that are affected by the annual cycle, most notably westerly wind bursts over the warm pool in the western equatorial Pacific in February-April, and from the perspective of the PDO, are essentially random and unpredictable (Kug et al.[11], Lengaigne et al. [12], [13]). The two main events in the PDO record over the past 60 years are the change in the mid 1970s, for which no satisfactory explanation exists, and the change in the late 1990s, which is apparently related to the large ENSO event in 1997/8. Both of these caused the system to move rapidly to a different state. As yet, no underlying low-frequency dynamical mechanism that can account for this variability has been identified (though creative suggestions have been made), and there is no confidence that any such exists. However, the PDO is important, and in any analysis of this nature it is always the second EOF after global warming.

3.3. EOF3: The Atlantic Meridional (Multidecadal) Oscillation

This pattern is normally termed the Atlantic Multi-decadal oscillation (the AMO). It is believed to be related to variations in the meridional overturning circulation due to sinking of dense water from the surface in the Greenland-Iceland-Norwegian Seas, and much of the evidence for this comes from modelling studies [1]. For this reason the term “meridional” is suggested here, as it conveys more information about its basis, and it is still the AMO. The conventional EOFs from both data sets are shown in Figure 7. Here there is general agreement between the two data sets about the main features of

the spatial pattern – generally, the Northern Hemisphere has a positive signal, and the Southern Hemisphere a negative one. There are some regional differences in the equatorial eastern Pacific and in the northwest Pacific. The time series contain a number of significant features, and these are mostly common to both records. Again, there is little difference between the analyses with and without the Southern Ocean. The signal is strongest in the Atlantic, in contrast to EOFs 1 and 2. The corresponding complex EOF (CEOF2) for HadISST1 is shown in Figure 8, with the time series on the complex plane in Figure 9. Here the real component is dominant (and most resembles real EOF3), with variance 0.73, with the imaginary part having variance 0.27. In Figure 9 there is evidence of cyclical variations, but with no well-defined period. Some large changes have periods of about 15 years, and others of about 40 years. From coupled modelling studies (e.g. Knight et al. [14, 15], [1], [16]), the maximum transport in the overturning ocean circulation coincides (approximately) with the maximum SST in the northern North Atlantic (positive signal in the time series in Figures 7 and 8).

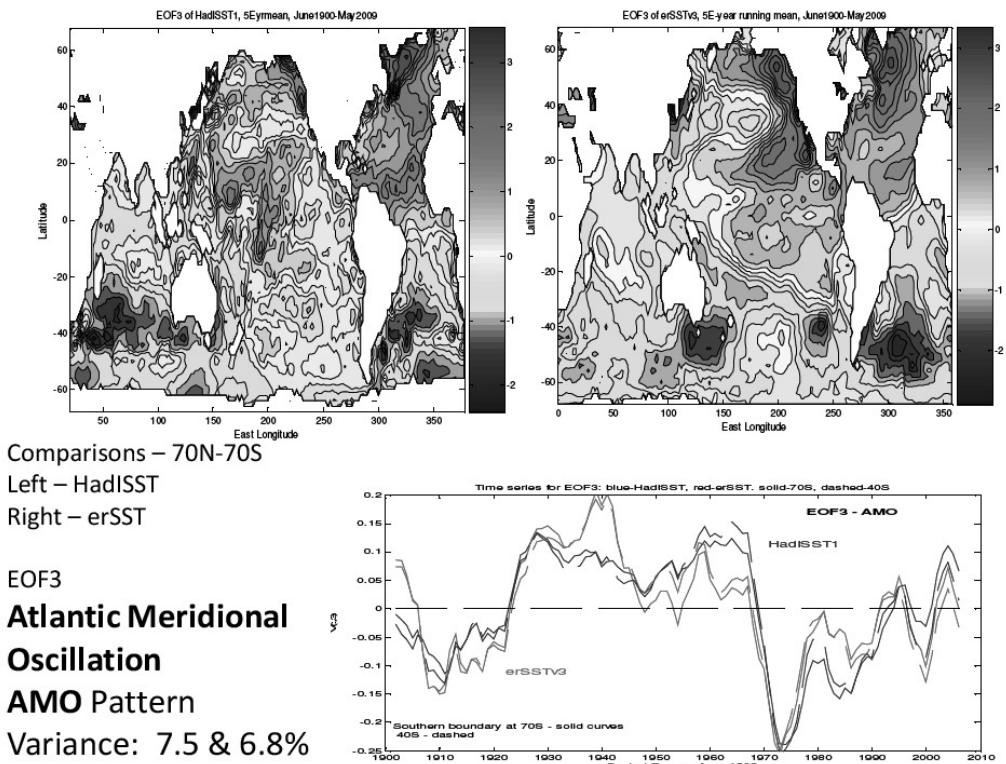

Fig. 7. As for Figure 2 but for the third EOF.

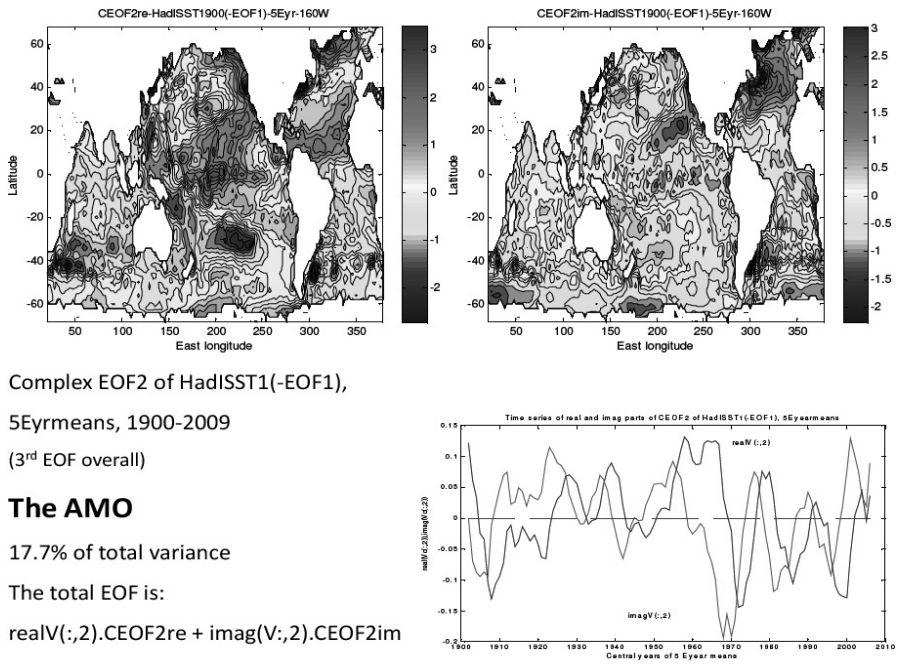

Fig. 8. As for Figure 5, but for the second complex EOF with the mean and EOF 1 removed.

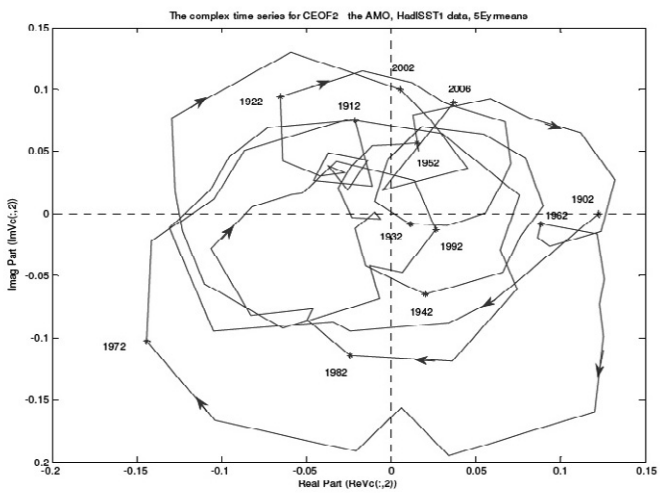

Fig. 9. As for figure 6, but showing the complex time series for CEOF2, mean and EOF1 removed.

The largest single event in the record is the change that occurred at the end of the 1960s. The working hypothesis here is that it is due to "natural" variations in the strength of the "Atlantic conveyor" as described above, but it may also be influenced by an increase in sulphate aerosol in the atmosphere in the Northern Hemisphere, due to the increase in industrial activity there between 1945 and 1970 (Baines and Folland [17]). This increases albedo and decreases surface temperature in the Northern Hemisphere, causing an asymmetric North-South Hemispheric response. For the ocean current transport in the Atlantic, the longest record of observations is that of transport through the Florida Straits, where reliable data exists back to the early 1960s. Figure 10 shows a plot of the 5-year running mean of this transport (from [18]), compared with the time series for the conventional EOFs of SST in Figure 7. The main point of comparison is the large change across the late 1960s, in both transport and SST patterns. Whatever, the cause of this event, the connection between ocean transport and this SST pattern seems real, with the transport reduction preceding the change in SST. The Florida current is only part of the total transport in the Atlantic, and it is dominated by the wind-driven component of the ocean circulation, but the general consistency seen here is encouraging.

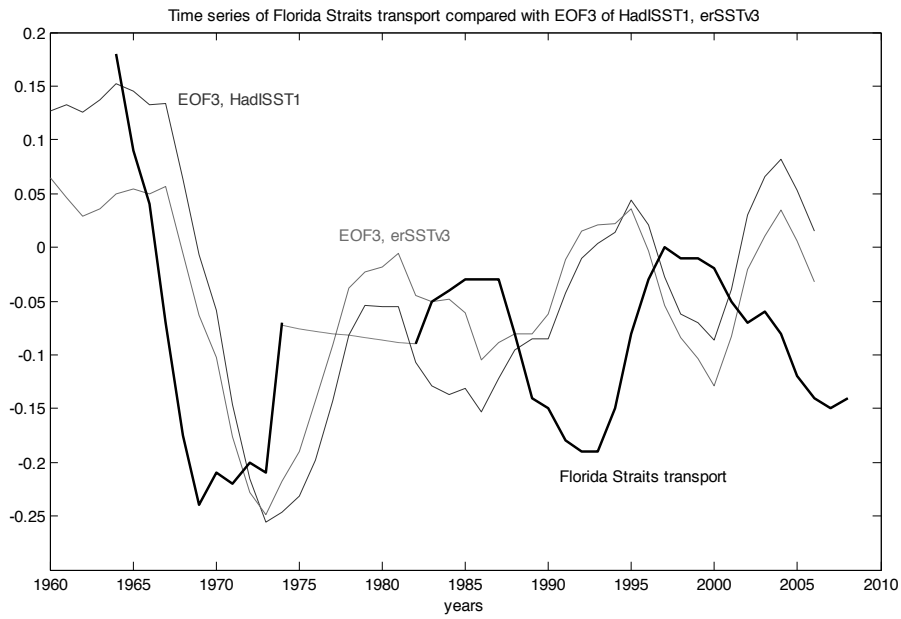

Fig. 10. The time series of the transport through the Florida Straits (black), compared with the time series of EOF3 for HadISST1 (blue), erSSTv3 (red) from Figure 7 (for latitude range 70N-40S). For the Florida current transport, the annual values denote 5-year running means (as for the SST), and one unit of scale is 10 Sverdrup, with the value zero at 33 Sverdrup. The dotted line denotes missing data. The Florida current data are from Meinen et al. [18].

3.4. EOF4: The Pacific Gyre Oscillation (PGO)

This pattern is related to the North Pacific Gyre Oscillation, described by di Lorenzo et al. [19]. The conventional EOFs are shown in Figure 11. There is clear and consistent (between the data sets) structure and in the North Pacific, where it resembles EOF2 of the North Pacific SST alone [19]. In the South

Pacific the pattern is quite different from that in the North, and there is some variation between the data sets. The structure in the Atlantic is the same for each data set, and differs from those of EOFs 1-3. There are differences in the Indian Ocean, but these are assumed here not to be important. The main features of all four time series are consistent. Figure 12 shows complex EOF3 for HadISST1. Here the dominant component is the imaginary part, for which the spatial pattern resembles (real) EOF4 with variance 0.59, whereas the real part has variance 0.41. The time series on the complex plane is shown in Figure 13. This indicates a dominant periodicity of the order of 40 years, but Figure 11 also indicates a component with period near 15 years.

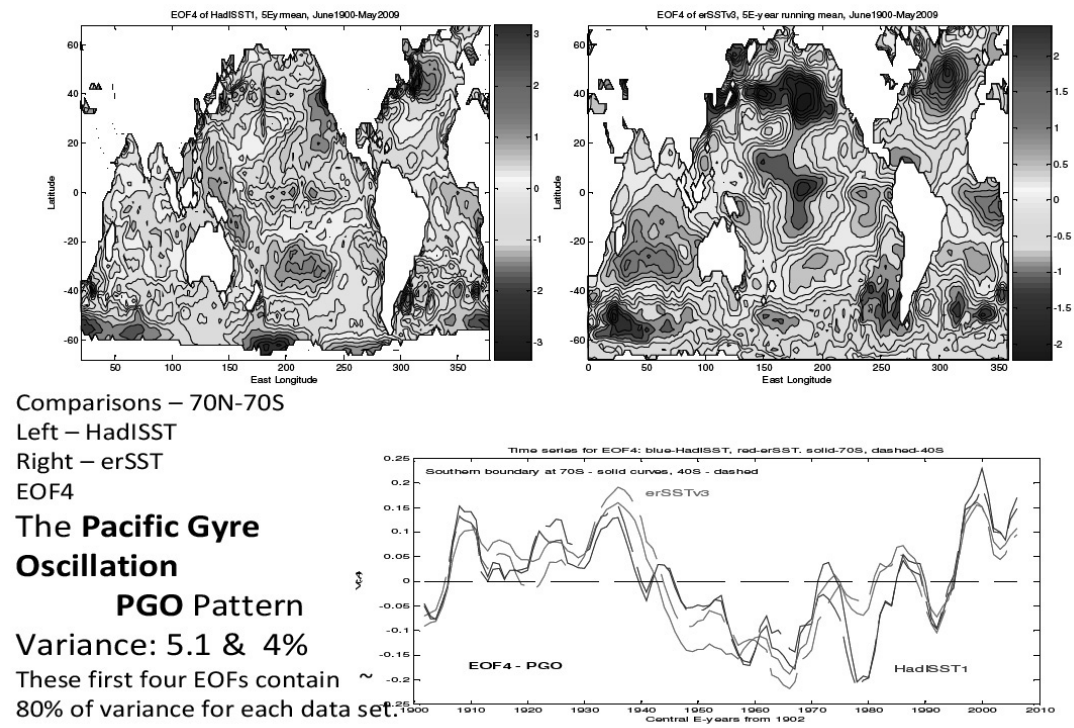

Fig. 11. The EOFs of HadISST1 and erSSTv3 as in Figure 2, but for EOF4.

This pattern is attributed to variations in the strength of the circulation in the North Pacific gyre [19], and presumably also on that in the South Pacific, the two circulations being linked in the tropics by the trade winds. A dynamical basis for these variations has been described by Latif and Barnett ([20-21]). They described a mechanism for decadal variability of the ocean circulation through its effect on the north/south SST gradient, and the effect of the latter in turn on the wind stress and wind stress curl, which drives the ocean circulation (a similar mechanism has been applied to the North Atlantic by Marshall et al. [22]). Fifteen-year fluctuations in the transport of the Kuroshio have been inferred from observational data since 1960 (Taguchi et al. [23]).

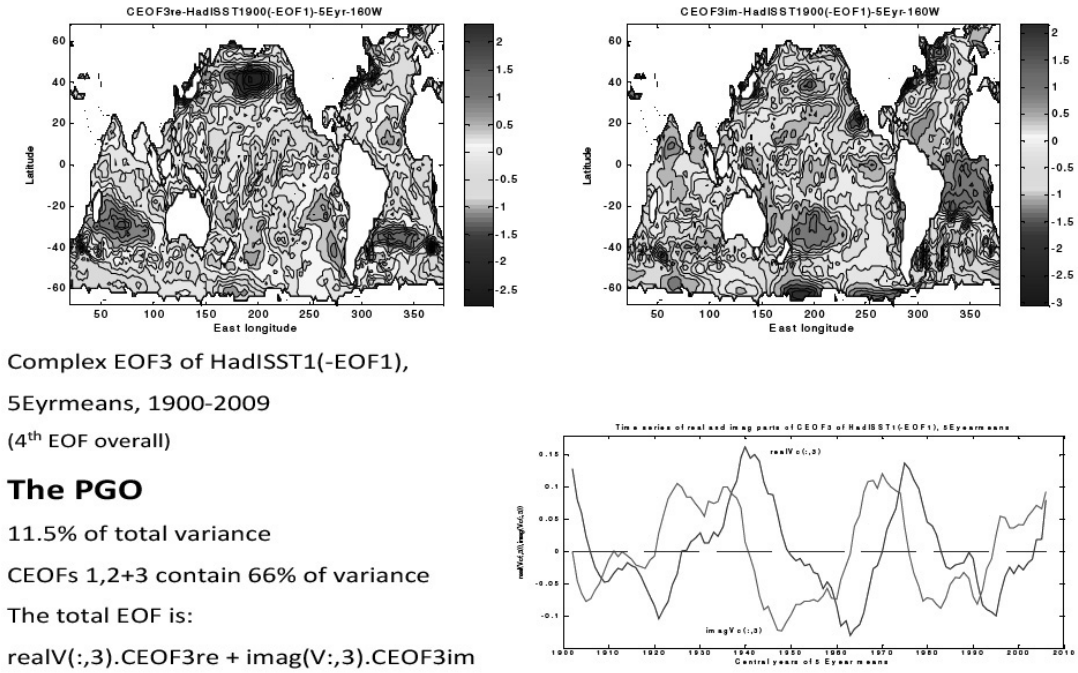

Fig. 12. As for Figure 5, but for the third complex EOF with the mean and EOF 1 removed, for HadISST1 data.

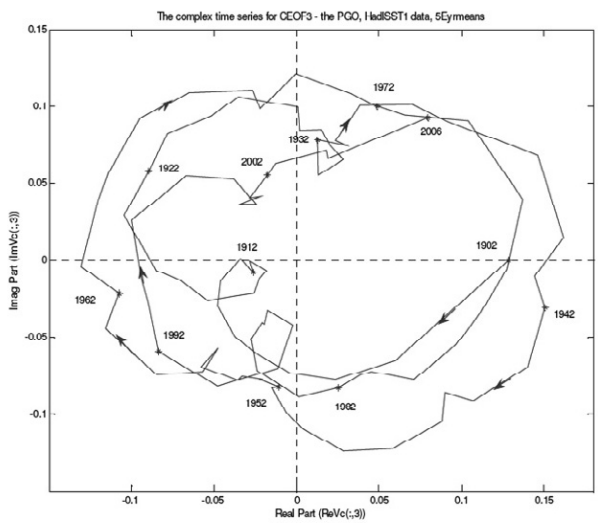

Fig. 13. As for figure 6, but showing the complex time series for CEOF3, mean and EOF1 removed, for HadISST1 data.

4. The relation to rainfall and other variables.

Since the time series of the real EOFs are mutually orthogonal, they may be used as bases for a breakdown of data from other variables. In principle, the same may be done with the complex time series of the CEOFs, but this is not pursued here. The time series (of either the EOFs or the CEOFs) may be projected onto the basic data to determine the degree of correlation, or to obtain the corresponding patterns in these other variables that accompany the patterns of the EOFs of interest. Most of these other variables have much shorter records than that of the SST. The past 30 (or so) years provide a rich and growing source of data from satellites and elsewhere, and it is useful to use the longer record of SST to examine these shorter records in order to evaluate the contributing factors in their variability. Here, one specific example of this application is given, to global rainfall over the past 30 years.

Global rainfall data are provided by the Global Precipitation Climatology Project (GPCP [24]), which combines rainfall data from a variety of sources and provides monthly mean rainfall. The latest version of this is termed GPCPv2.1. Here a conventional EOF analysis has been carried out on a 5-year running mean of these data. The first EOF (not shown) is clearly related to the ENSO phenomenon and has no secular trend. The second EOF is the principal interest here, and is shown in Figure 14 (bottom left). The time series of this EOF (red curve, bottom right) contains an upward secular trend since the early 1990s, and its spatial pattern shows stark changes in the pattern of global rainfall – a decrease in the equatorial west and central Pacific, an increase in the rest of the tropics and the southwest Pacific, and smaller but significant changes in mid-latitudes (including rainfall decrease in Southwest Australia and the United States). EOF1 of a similar analysis of the two SST data sets (over slightly more years, since they are available) have very similar time series, containing the secular trend, and these are also shown in Figure 14. Higher order EOFs of any of these three data sets do not contain any long-term trend as is seen here. Further, if the analysis is repeated for other relevant atmospheric variables, such as surface winds, or vertical velocity at mid-troposphere levels, a corresponding "trend" EOF arises with the same trend in its temporal structure. Accordingly, this trend pattern constitutes a coordinated behaviour of the whole system, which may be characterized by the patterns of SST. We may therefore take the two SST patterns as two representations of this trend pattern of behaviour, and ask the question: to what extent do the patterns and processes identified by EOFs of the long-term SST data records in the previous section contribute to this recent trend?

We may estimate the various contributions of the long-term SST EOFs by writing the 28-year trend as

$$S_{28}(1,1)U_{28}(:,1)V_{28}(:,1), \tag{3}$$

and the 105-year EOFs as

$$\sum_{n=1}^{N} S_{105}(n,n)U_{105}(:,n)V_{105}(:,n) \tag{4}$$

in the notation of section 2. Each of the terms in the series (4) is then projected onto the expression (3), by taking the dot product of both the spatial patterns and the time series of these terms. In other words, in estimating the contribution of each term in (4) to (3), both the spatial patterns and the time series are compared. The results are given in Table 1. For the HadISST1 data, the trend pattern is distributed amongst the four basic patterns, but for the erSSTv3 data, it is mostly concentrated between the first two – global warming, and the Pacific Decadal Oscillation. This disagreement is disappointing, given the apparent agreement between the two SST data sets shown for each of the four main basic patterns. However, it does imply that global warming and the PDO are principal causes of the pattern of the trend in rainfall over the past 15 years.

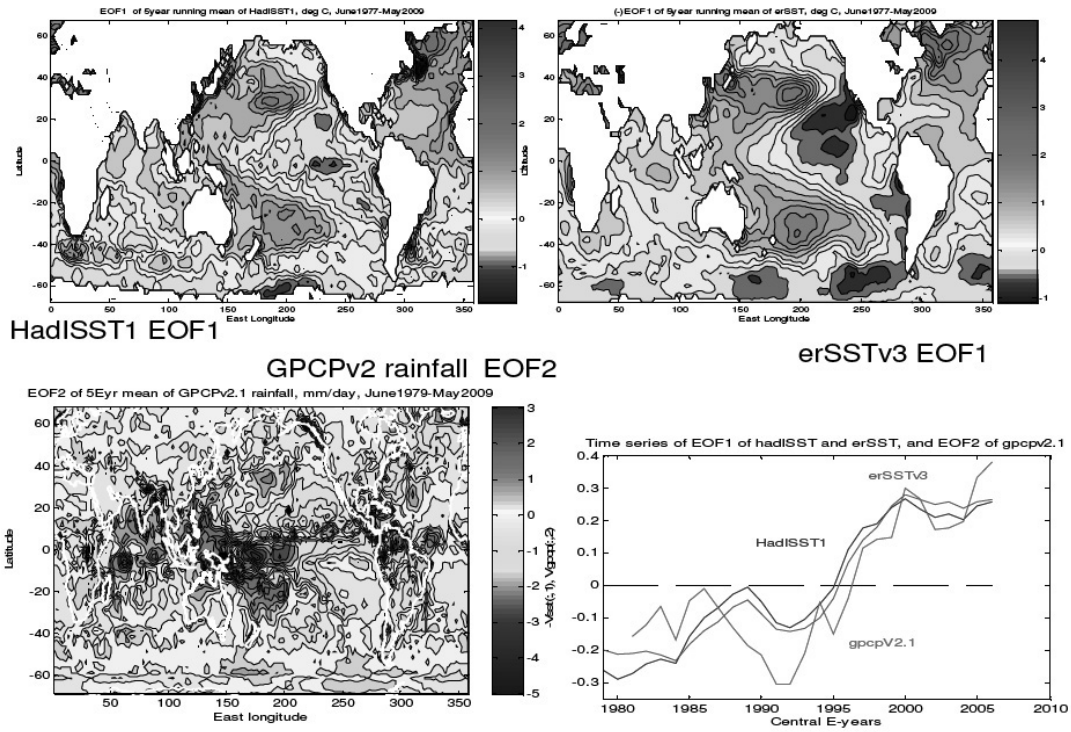

Fig. 14. EOF1 of 5-year running means since 1979 for HadISST1(top left) erSSTv3 (top right), EOF2 of GPCPv2.1 rainfall (bottom left). The time series of all three are superimposed (bottom right), blue denoting HadISST, green: erSST, red: GPCP rainfall.

Table 1. Contributions to the trend EOF over the past 30 years from each of the EOFs of the long-term SST analysis, from the two data sets.

	105-year EOF1 GW	**EOF2** PDO	**EOF3** AMO	**EOF4** PGO	**EOF5**
For HadISST1:					
1	0.357	0.17	0.124	0.265	0.02
100%	26%	17%	12%	27%	2%
For erSSTv3:					
1	**0.319**	**0.385**	**0.002**	**0.041**	**0.125**
100%	**32%**	**39%**	**0**	**4%**	**13%**

5. Conclusions.

From an analysis of sea surface temperature and additional data, the principal global patterns of climate variability on the decadal time scale have been described and summarized. These patterns may be termed: (1) the global warming (GW) pattern, (2) the Pacific Decadal Oscillation (PDO) pattern, (3) the Atlantic Multidecadal Oscillation (AMO) pattern, and (4) the Pacific Gyre Oscillation (PGO) pattern. In the case of patterns 2, 3 and 4, they are based in a particular ocean, but their principal features may carry over into other oceans at the same latitude by atmospheric advection. Each of these patterns is associated with a different set of physical/dynamical processes. Detailed data with sufficiently long records to describe and confirm the main aspects and dynamics of these patterns are still lacking, and some may prefer to regard the dynamical scenarios described here as hypothetical. I believe, however, that the case is much stronger than this, that these patterns are coming into focus, and that it is helpful to attempt to fit climate variability on the scale of 10-100+ years into the framework that I have described. The data also suggest the possibility of a fifth global pattern, but so far there is no indication as to what its physical basis might be.

If the above decomposition of patterns is accepted, the connection with other variables such as rainfall and descriptors of the biosphere may be analysed by projecting (regressing) the principal time series that characterize these patterns onto these variables. These decadal variability patterns have been applied here to the recent trend in global rainfall, with the objective of inferring the processes that may cause it. The results have been only partially successful, as the two SST data sets do not agree on the distribution between the patterns. This is disappointing, and suggests that the optimum representation of the historical record of global SST has yet to be realized. However, they do agree that both global warming and the Pacific Decadal Oscillation are major contributors to the current rainfall trend.

References

[1] Parker D, Folland F, Scaife A, Knight J, Colman A, Baines P, Dong B. Decadal to multidecadal variability and the climate change background. *J. Geophys. Res* 2007: **112**: D18115, doi:10.1029/2007JD008411, 2007.

[2] Rayner NA, Parker DE, Horton EB, Folland CK, Alexander LV, Rowell DP, Kent EC, Kaplan A. Global analyses of sea surface temperature, sea ice, and night marine airtemperature since the late nineteenth century. *J. Geophys. Res.* 2003;**108,** 4407, doi:10.1029/2002JD002670.

[3] Smith TM, Reynolds RW, Peterson TC, Lawrimore J. Improvements to NOAA's Historical Merged Land-ocean Surface Temperature Analysis (1880-2006). *J. Climate* 2008; **21**: 2283-2296.

[4] Kaplan A, Cane MA, Kushnir Y, Clement, AC, Blumenthal MB, Rajagopalan B. Analyses of global sea surface temperature 1856-1991. *J. Geophys. Res.* 1998;**103**(C9): 18567-18589.

[5] Kaiser HF. The Varimax Criterion for analytic rotation in factor analysis. *Psychometrika* 1958;**23**: 187-200.

[6] IPCC 2007 Intergovernmental Panel on Climate Change, 4th Assessment Report. www.ipcc.ch.

[7] Thompson DWJ, Kennedy JJ, Wallace JM, Jones, PD A large discontinuity in the mid-twentieth century in observed global-mean surface temperature. *Nature* 2008;**453**: 646-649.

[8] Lyman JM, Good SA, Gouretski VV, Ishii M, Johnson GC, Palmer MD, Smith DM, Willis JK. Robust warming of the global upper ocean. *Nature* 2010; **465**: 334-337.

[9] Mantua NJ, Hare SR, Zhang Y, Wallace JM, Francis RC. A Pacific interdecadal climate oscillation with impacts on salmon production. *Bull. Amer. Meteorol. Soc*. 1997; **78**: 1069-1079.

[10] Power S, Casey T, Folland C, Colman A, Mehta, V. Inter-decadal modulation of the impact of ENSO on Australia, *Climate Dynamics* 1999;**15**: 319-324.

[11] Kug JS, Jin FF. An SI, Two types of El Niño events: cold tongue El Niño and warm pool El Niño. *J. Clim*. 2009;**22**: 1499-1515.

[12] Lengaigne M, Guilyardi E, Boulanger JP, Menkes C, Delecluse P, Inness P, Cole J, Slingo J. Triggering of El Niño by westerly wind events in a coupled general circulation model, *Climate Dynamics* 2004; **23**:601-620.

[13] Lengaigne M, Boulanger JP, Menkes C. Spencer H. Influence of the seasonal cycle on the termination of El Niño events in a coupled general circulation model. *J. Clim.* 2006; **19**:1850-1868.
[14] Knight JR, Allan RJ, Folland CK, Vellinga M, Mann ME. A system of persistent natural thermocline circulation cycles in observed climate. *Geophys. Res. Lett.,* 2005; **32**: L20708, doi:10.1029/2005GL024233.
[15] Knight JR, Folland CK, Scaife AA. Climate impacts of the Atlantic Multidecadal Oscillation. *Geophys. Res. Lett*. 2006; **33**:L17706, doi:10.1029/2006GL026242.
[16] Knight JR. The Atlantic Multidecadal Oscillation inferred from the forced climate response in coupled general circulation models. *J. Clim.* 2009; **22**: 1610-1625.
[17] Baines PG, Folland CK. Evidence for a rapid global climate shift across the late 1960s. *J. Clim.* 2007; **20**: 2721-2744.
[18] Meinen CS, Bollinger MO, Garcia RF. Florida current transport variability: An analysis of annual and long-period signals. *Deep-Sea Res*. I 2010; **57**: 835-846.
[19] Di Lorenzo E, Schneider N, Cobb KM, Franks PJS, Chhak K, Miller AJ, McWilliams JC, Bograd SJ, Arange H, Curchitser E, Powell TM, Riviére, P. North Pacific Gyre Oscillation links ocean climate and ecosystem change. *Geophys. Res. Lett*. 2008; **35** :L08607, doi:10.1029/2007GL032838, 2008.
[20] Latif M, Barnett K, Causes of decadal climate variability over the North Pacific and North America. *Science* 1994;**266**:634-637.
[21] Latif, M. and Barnett, K. Decadal climate variability over the North Pacific and North America: dynamics and predictability. *J. Clim*. 1996; **9**: 2407-2423.
[22] Marshall J, Johnson H, Goodman J. A study of the interaction of the North Atlantic Oscillation with ocean circulation. *J. Clim*. 2001; **14**:1399-1421.
[23] Taguchi B, Xie SP, Schneider N, Nonaka M, Sasakei H, Sasai Y. Decadal variability of the Kuroshio extension: observations and an eddy-resolving model hindcast. *J. Clim*. 2007: **20**: 2357-2377.
[24] Adler RF, Huffman GJ, Chang A, Ferraro R, Xie P, Janowiak J, Rudolf B, Schneider U, Curtis S, Bolvin D, Gruber A, Susskind J, Arkin P, Nelkin E. The Version 2 Global Precipitation Climatology Project (GPCP) Monthly Precipitation Analysis (1979-Present). *J. Hydrometeor*. 2003;**4**:1147-1167.